Journal of Solid State Chemistry **152,** 478–485 (2000)
doi:10.1006/jssc.2000.8716, available online at http://www.idealibrary.com on IDEAL®

Crystal Structure and Bonding in the Rare-Earth Rich Ternary Pnictides RE_5M_2X (RE = Y, Gd, Tb, Dy, Ho, Er, Tm, Lu; M = Ni, Pd; X = Sb, Bi)

Yurij Mozharivskyj and Hugo F. Franzen[1]

Department of Chemistry and Ames Laboratory of U.S. DOE, Iowa State University, Ames, Iowa 50011

Received January 19, 2000; in revised form February 29, 2000; accepted March 10, 2000

Eleven new rare-earth antimonides and bismuthides RE_5M_2X (see Table 1) have been synthesized and characterized by X-ray powder methods. The compounds are isostructural to the previously reported pnictides RE_5M_2X and adopt the Mo_5B_2Si structure (space group *I*4/*mcm*, an ordered version of Cr_5B_3). Atomic and thermal parameters have been refined for Ho_5Ni_2Sb and Ho_5Ni_2Bi. Extended Hückel tight-binding calculations performed on Y_5Ni_2Sb show strong Y–Ni, Y–Sb, and Y–Y interactions. © 2000 Academic Press

1. INTRODUCTION

Investigation of ternary rare-earth transition metal antimonides and bismuthides has been growing over the last two decades. The interest in this field is prompted by the search for new magnetic materials (1–4) and by attempts to synthesize new compounds and to understand their chemistry (5). Exchanging a rare-earth element allows tracking steric factors in the structures (4, 6). An increase in atomic radii normally leads to a larger unit cell, but it may also result in the change of the structure type: *RE*NiSb (*RE* = La, Ce, Pr, Nd, Sm) crystallizes with ZrBeSi structure, while the antimonides of the heavy rare earths (Gd–Lu) adopt the MgAgAs structure (4). On the other hand, substitution of a transition metal results in subtle electronic effects (7, 8) that determine the structure and homogeneity ranges for the structure. Varying composition not only results in different structures but also leads to different spatial arrangements of building units: compounds with a high amount of antimony adopt one- or two-dimensional structures (1–3, 5, 9–11) whereas antimonides richer in a rare-earth or transition metal are normally three-dimensional (2, 4, 6, 12, 13). Crystal structures of the bismuthides (8, 14) are similar to those of the antimonides, but there are few known compounds.

The studies in the rare-earth transition metal antimonide and bismuthide systems have been mainly focused on the region with relatively high (over 30 at%) amounts of antimony or bismuth. Considering the variety of binary rare-earth rich phases, one can expect new compounds to exist in the rare-earth rich regions. Recently synthesized pnictides RE_5M_2X (RE = Y, Gd–Lu except Yb; M = Ni, Pd; X = Sb, Bi) (13, 15, 16) extended the number of the known rare-earth rich phases, which were, until recently, limited to those of the RE_5CuBi_3-type (17). Greater rare-earth content and the presence of a late transition metal, as opposed to a metalloid, in the RE_5M_2X phases dictates increased metal–metal interaction.

Combination of the early transition metal or *f*-elements with late transition metals could be considered as a Lewis acid–base reaction and could lead to the formation of the strong intermetallic bonds. The extra stability of such polar interactions was first noted by Brewer and Wengert (18) who proposed that for a fourth group element, such as zirconium, the maximum in stability should be with iridium or platinum. For a third group metal, such as yttrium, the maximum interaction would be expected at platinum. The significance of these bonds can be seen in the surrounding of the atoms and structural motif of the early late-transition metal compounds. In the late-transition metal poor phases, such as Hf_5MTe_3 (19), Zr_6MTe_2 (20), $Zr_9Ni_2P_4$ (21), and $Ta_9M_2S_6$ (22), these bonds take precedence over the interactions between the late transition metal (M) and main group element. Mixed-metal features in pnictides and chalcogenides are largely trigonal prisms of the earlier transition metal or *f*-elements centered by a late transition metal: Zr_6Co in Zr_6CoAs_2 (23), Hf_6Ni in $Hf_6Ni_{1-x}Sb_{2+x}$ (24), Sc_6Ni in $Sc_5Ni_2Te_2$ (25), Ta_6M (M = Fe, Co, Ni) in $Ta_9M_2S_6$ (22), and RE_6M in RE_5M_2X (13, 15, 16). Mulliken overlap population (MOP) indicates that in the ternary compounds with a main group element such mixed-metal

[1] To whom correspondence should be sent. E-mail: franzen@ameslab.gov.

0022-4596/00 $35.00

bonds can be as strong as in the binary mixed metal compounds (26). Also the strength of the interaction between early transition metal atoms is comparable to those in the pure elements (24). As a result separate clusters or one-, two-, and three-dimensional frames of the early-transition metals can be formed, depending on the number of metal-based electrons. In Ta_2S and Ta_6S (27) the Ta atoms form chains of the fused pentagonal antiprisms, in $Hf_5Co_{1+x}P_{3-x}$ (28, 29) the Hf atoms constitute double hexagonal channels, and in Hf_2NiP (30) the Hf atoms form 2D zigzag nets with weak bonding between them.

In the present paper we consider the metal–metal bonding in the rare-earth rich ternary pnictides, extending the ideas of the interaction from the early late-transition metal compounds to the phases with rare-earth metals (*f*-elements) and nickel or palladium.

2. EXPERIMENTAL PROCEDURES

2.1. Syntheses

The starting materials were ingots of *RE* elements (with purity not less than 99.8%), antimony (99.99%, Johnson Matthey GmbH), bismuth (99.999%, ChemPur), nickel (99.99%, ChemPur), and palladium (99.9%, Merck KGaA). The mixtures of the components with the initial compositions RE_5M_2X and with a total weight of 1 g were arc-melted in an argon atmosphere and were then turned over and remelted to reach homogeneity. The samples were sealed in evacuated silica tubes, annealed at 800°C for 10 days, and then furnace-cooled.

2.2. Structure Analysis

The data for the new pnictides RE_5M_2X (see Table 1) were collected using Siemens D5000 (Cu$K\alpha_1$ radiation) and Scintag (Cu$K\alpha_1$ and Cu$K\alpha_2$ radiation, cooled solid-state detector) powder diffractometers. The patterns revealed the new phases to be isostructural with the known RE_5M_2X compounds. The CSD (31) program package was used to describe the peak profiles and determine their 2θ angle values, and the lattice parameters were derived by the least-squares procedure (Table 1).

The structures of Ho_5Ni_2Sb and Ho_5Ni_2Bi were refined by the Rietveld method (Fig. 1, program FullProf (32)). The final *R* factors as well as the details relevant to the data collections and refinements are compiled in Table 2. Atomic and isotropic thermal parameters are given in Table 3, and interatomic distances are presented in Table 4.

During the refinement of erbium nickel bismuthide (15) a large temperature factor was observed for the Ni atoms. During the final steps of the refinement the occupancy factor for Ni was allowed to deviate from unity which led to the Ni deficiency ($Er_5Ni_{1.72(4)}Bi$) and to a lower *R*-value. On the basis of this finding for the Er compound, partial occupancies were assigned to the other rare-earth nickel bismuthides (15), but the refinement of Ho_5Ni_2Sb and Ho_5Ni_2Bi (this work) did not yield a Ni deficiency for these compounds. For Ho_5Ni_2Sb and Ho_5Ni_2Bi the temperature factors of the Ni atoms were even lower than for the other elements, which was a convincing argument for the Ni position being fully occupied. So only $Er_5Ni_{1.72(4)}Bi$ was found to occur with a Ni deficiency (Table 1), while all other pnictides were assumed to have the ideal composition RE_5M_2X. However, this assumption does not rule out a Ni deficiency in other compounds, and a possible deviation from the composition RE_5M_2X must be checked for each pnictide individually, when needed.

Small differences between the lattice parameters for Ho_5Ni_2Sb and Ho_5Ni_2Bi, previously reported (13, 15) and

TABLE 1
Lattice Parameters of the RE_5M_2X Pnictides

Compound	*a*, Å	*c*, Å	*c*/*a*	*V*, Å^3	Reference
Y_5Ni_2Sb	7.662(3)	13.502(9)	1.762	792.7	13
Gd_5Ni_2Sb	7.698(3)	13.403(9)	1.741	794.3	This work
Tb_5Ni_2Sb	7.641(2)	13.266(5)	1.736	774.5	13
Dy_5Ni_2Sb	7.593(2)	13.258(5)	1.746	764.4	13
Ho_5Ni_2Sb[a]	7.563(1)	13.250(3)	1.752	757.9	13
Er_5Ni_2Sb	7.531(2)	13.178(7)	1.750	747.4	13
Tm_5Ni_2Sb	7.459(3)	13.252(9)	1.777	737.3	This work
Lu_5Ni_2Sb	7.429(2)	13.190(8)	1.775	728.0	13
Y_5Ni_2Bi	7.673(2)	13.566(5)	1.768	798.7	15
Gd_5Ni_2Bi	7.756(2)	13.537(6)	1.745	814.3	15
Tb_5Ni_2Bi	7.693(2)	13.445(6)	1.748	796.0	15
Dy_5Ni_2Bi	7.651(4)	13.450(9)	1.758	787.3	15
Ho_5Ni_2Bi[a]	7.624(4)	13.420(6)	1.760	780.0	15
$Er_5Ni_{1.72(4)}Bi$	7.5813(9)	13.395(2)	1.767	769.8	15
Tm_5Ni_2Bi	7.522(4)	13.411(8)	1.783	758.8	15
Lu_5Ni_2Bi	7.429(2)	13.415(9)	1.806	740.3	15
Y_5Pd_2Sb	7.733(1)	13.582(5)	1.756	812.2	16
Gd_5Pd_2Sb	7.812(3)	13.645(7)	1.747	832.7	This work
Tb_5Pd_2Sb	7.730(2)	13.508(5)	1.747	807.1	16
Dy_5Pd_2Sb	7.715(2)	13.507(4)	1.750	804.0	16
Ho_5Pd_2Sb	7.6795(7)	13.476(8)	1.755	794.7	16
Er_5Pd_2Sb	7.641(4)	13.465(9)	1.762	786.2	16
Tm_5Pd_2Sb	7.585(2)	13.457(6)	1.774	774.2	16
Lu_5Pd_2Sb	7.5531(8)	13.345(2)	1.767	761.3	16
Y_5Pd_2Bi	7.779(1)	13.699(5)	1.761	829.0	This work
Gd_5Pd_2Bi	7.864(2)	13.644(4)	1.735	843.8	This work
Tb_5Pd_2Bi	7.820(1)	13.585(2)	1.737	830.8	This work
Dy_5Pd_2Bi	7.770(2)	13.558(5)	1.745	818.5	This work
Ho_5Pd_2Bi	7.719(1)	13.563(5)	1.757	808.1	This work
Er_5Pd_2Bi	7.695(1)	13.527(4)	1.758	801.0	This work
Tm_5Pd_2Bi	7.652(1)	13.474(4)	1.761	788.9	This work
Lu_5Pd_2Bi	7.586(2)	13.440(6)	1.772	773.4	This work

[a] Lattice parameters from the Rietveld refinement (this work) are given in Table 2.

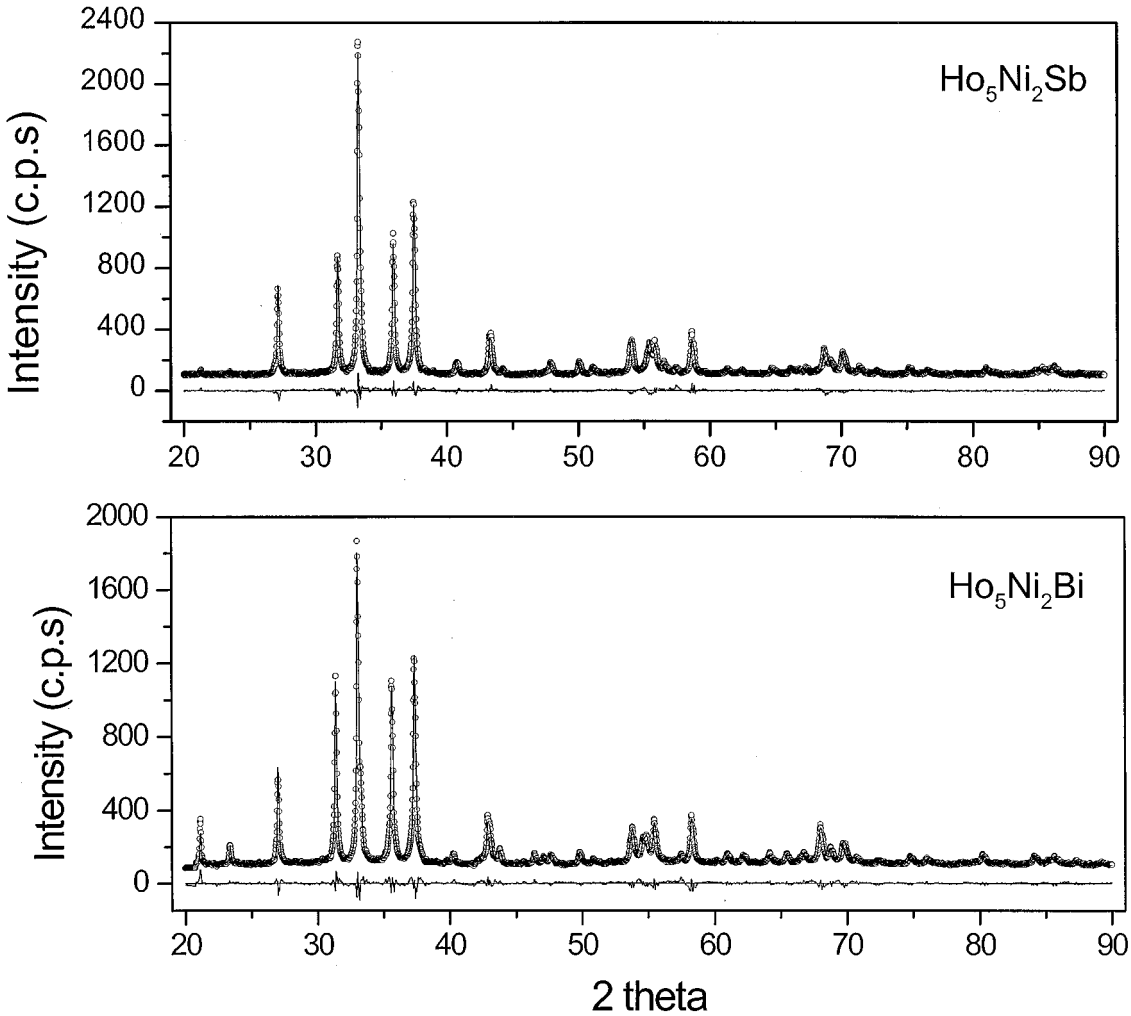

FIG. 1. Observed (circles) and calculated (solid line) profiles and differences between them for Ho_5Ni_2Sb and Ho_5Ni_2Bi.

obtained by the Rietveld method, are due to variations in the sample preparation, treatment, and equipment used.

2.3. Band Structure Calculations

Band structure calculations were performed by the extended Hückel tight-binding (EHTB) method (33). To simplify calculations the antimonide Y_5Ni_2Sb, which does not require using *f*-orbitals, was chosen for an electronic structure characterization. Y_5Ni_2Sb, instead of Ho_5Ni_2Sb, is also the preferred choice because there are no well-tabulated atomic data for holmium for extended Hückel calculations. Atomic coordinates in Y_5Ni_2Sb were assumed to be the same as in refined Ho_5Ni_2Sb (Table 3). This assumption can be justified by similarity in the atomic coordinates of Ho_5Ni_2Sb and previously reported Gd_5Ni_2Sb (13) and by the fact that yttrium is close both crystallographically and chemically to the Gd–Lu lanthanoids.

The orbital energies and coefficients for the Slater-type orbitals were taken from (34). The parameters of Y and Ni were then refined by the alternating charge iteration technique, while the Sb parameters were kept constant (Table 5).

3. RESULTS AND DISCUSSION

3.1. Structure Description

The RE_5M_2X compounds (Fig. 2) crystallize with the Mo_5B_2Si-type (35, 36) structure that is an ordered version of Cr_5B_3 in which the boron atoms occupy the two point positions 4(*a*) and 8(*h*). Distribution of the *M* and *X* atoms in RE_5M_2X (also the B and Si atoms in Mo_5B_2Si) on the boron sites in Cr_5B_3 obeys the stoichiometry as well as the size factor (13). More detailed structural description of the compounds depends on whether the electronic properties or the structural relationship to other compounds is to be emphasized. Traditionally, structures have been described

TABLE 2
Collection and Refinement Data for Ho_5Ni_2Sb and Ho_5Ni_2Bi

	Ho_5Ni_2Sb	Ho_5Ni_2Bi
Space group (Pearson symbol)	*I*4/*mcm* (*tI*32)	*I*4/*mcm* (*tI*32)
Lattice parameters, Å	$a = 7.5793(3)$	$a = 7.6140(3)$
	$c = 13.2864(6)$	$c = 13.4435(6)$
Diffractometer	Scintag	Scintag
Wavelength	$CuK\alpha_1$ and $CuK\alpha_2$	$CuK\alpha_1$ and $CuK\alpha_2$
2θ and step	20–90°, 0.02°	20–90°, 0.02°
No. of reflections	188	192
No. of fitted parameters	19	15
$R_P = \sum\|y_{oi} - y_{ci}\|/\sum\|y_{oi}\|$	0.0636	0.0652
$R_{wP} = (\sum w_i(y_{oi} - y_{ci})^2/\sum w_i(y_{oi})^2)^{1/2}$ [a]	0.0811	0.0856
$R_I = \sum\|I_o - I_c\|/\sum\|I_o\|$	0.0680	0.0348
$R_F = \sum\|F_o - F_c\|/\sum\|F_o\|$	0.0770	0.0318

[a] $w_i = (y_{oi})^{-1/2}$.

TABLE 4
Interatomic Distances (Å) in Ho_5Ni_2Sb and Ho_5Ni_2Bi

Atoms	Ho_5Ni_2Sb	Ho_5Ni_2Bi	Atoms	Ho_5Ni_2Sb	Ho_5Ni_2Bi
Ho1–4Ni	2.961(4)	2.989(4)	Ho2–1Ho2	3.689(2)	3.690(3)
2*X*[a]	3.3216(6)	3.3609(6)	2Ho2	3.802(2)	3.847(2)
8Ho2	3.400(1)	3.419(1)			
			Ni–1Ni	2.842(6)	2.786(6)
Ho2–2Ni	2.879(4)	2.854(4)	4Ho2	2.879(4)	2.854(4)
1Ni	2.906(4)	2.962(4)	2Ho2	2.906(4)	2.962(4)
2*X*	3.215(1)	3.253(1)	2Ho1	2.961(4)	2.989(4)
1Ho2	3.386(2)	3.348(2)			
2Ho1	3.400(1)	3.419(1)	*X*–8Ho2	3.215(1)	3.253(1)
1Ho2	3.553(2)	3.652(2)	2Ho1	3.3216(6)	3.3609(6)

[a] *X* = Sb or Bi.

in terms of coordination polyhedra (37, 38). These polyhedra may be then oriented in various ways and connected via corners, edges, or faces. This approach allows visualization of coordination spheres and rationalizes bonding between the central atom and its close neighbors. Another concept describes crystal structures in terms of stacked layers, focusing on the atom connectivity. In this light, the structure of Ho_5Ni_2Sb (Fig. 2) can be built from Ho2 3^2.4.3.4 networks, known as an Archimedean tiling. There are four such layers per unit cell, two of them (*A*) are rotated at 45° to the other two (*B*) (Fig. 2), and their stacking order along the *c* direction is *AABBAA*. Separation between the same tilings in Ho_5Ni_2Sb is 3.689 Å, and the distance between the different tilings is only 2.954 Å. Superimposing the same two 3^2.4.3.4 networks (*A* or *B*) produces voids in the shape of trigonal and tetragonal prisms, while combination of two different networks $A + B$ forms tetrahedra and tetragonal antiprisms (Archimedian cubes). Small Ni atoms center the small trigonal prisms, larger Sb atoms center the tetragonal antiprisms, and the Ho1 atoms are in the tetragonal prisms (Fig. 3). Now, the structure can be alternatively viewed as the stacking of two slabs in the *c* direction, one (*I*) being made of filled face-sharing trigonal and tetragonal prisms, the other (*II*) of empty tetrahedra and filled edge-sharing tetragonal antiprisms.

Inserting Ni atoms in the small trigonal prisms of slab *I* results in Ho–Ni distances (Fig. 3 and Table 4) which are shorter than the sum of the metallic radii $r_{Ho} + r_{Ni} = 1.743 + 1.246 = 2.989$ Å. Antimony or bismuth atoms, located in large tetragonal antiprisms of slab *II*, do not interact strongly with eight Ho neighbors at distances of 3.215 and 3.253 Å. There is variety of Ho–Ho distances in the structure, but only one Ho2–Ho2 bond in the 3^2.4.3.4 network is of particular interest. These two atoms are shared by two base-fused triangles in the 3^2.4.3.4 tiling and they belong to two different tetragonal antiprisms in slabs *II* (Fig. 3). This interatomic distance is quite short (3.386 Å) in Ho_5Ni_2Sb, but it is even shorter (3.348 Å) in the larger Ho_5Ni_2Bi. The same trend is observed for the Ni–Ni interactions and one of Ni–Ho2 bonds. This is opposite to what one would expect from the substitution of Sb atoms by larger Bi atoms. Thus, a more detailed analysis of the structure is instructive.

Introducing Bi atoms in place of Sb atoms in the tetragonal antiprisms results in a larger volume and larger distances between the atoms forming the antiprism. Inflating the volume shortens the distances between Ho2 atoms, which

TABLE 3
Atomic and Isotropic Thermal (B_{iso}, Å^2) Parameters for Ho_5Ni_2Sb and Ho_5Ni_2Bi (Space Group *I*4/*mcm*, Mo_5B_2Si Structure Type)

		Ho_5Ni_2Sb				Ho_5Ni_2Bi			
Atom		*x*	*y*	*z*	B_{iso}	*x*	*x*	*z*	B_{iso}
Ho1	4*c*	0	0	0	2.71(13)	0	0	0	1.47(13)
Ho2	16*l*	0.1579(2)	$x + 1/2$	0.1388(1)	3.03(6)	0.1555(2)	$x + 1/2$	0.1372(1)	1.22(4)
Ni	8*h*	0.3675(6)	$x + 1/2$	0	2.29(14)	0.3706(6)	$x + 1/2$	0	0.58(14)
X	4*a*	0	0	1/4	2.66(14)	0	0	1/4	0.80(7)

TABLE 5
Parameters for the Extended Hückel Tight-Binding Calculations

Atom	Orbital	H_{ii}, eV	ξ_1	c_1[a]	ξ_2	c_2[a]
Y	5*s*	−6.82	1.39	1.00		
Y	5*p*	−4.30	1.39	1.00		
Y	4*d*	−6.56	4.33	0.5657	1.06	0.6575
Ni	4*s*	−6.83	1.825	1.00		
Ni	4*p*	−3.35	1.125	1.00		
Ni	3*d*	−9.76	5.75	0.5683	2.00	0.6292
Sb	5*s*	−18.80	2.323	1.00		
Sb	5*p*	−11.70	1.999	1.00		

[a] Coefficients used in the double-zeta Slater-type orbitals.

belong to the neighboring antiprisms and form a base of the triangles in $3^2.4.3.4$ network. Shorter bases result in the shorter Ni–Ho2 distances and Ni atoms from the face-sharing trigonal prisms come closer. Other distances undergo a small increase in Ho_5Ni_2Bi as expected.

Table 1 presents lattice parameters for RE_5M_2X and Fig. 4 shows changes in unit cell volumes versus atomic number. The Pd compounds have larger *a* and *c* constants than the corresponding Ni compounds. The volume of all pnictides decreases gradually with the atomic number of the rare earth and the plots reflect the well-known lanthanide contraction. We were not able to synthesize similar compounds with the lighter rare earths or with ytterbium. The absence of Yb compounds in the series might be explained by its mixed valence and larger atomic radius.

3.2. Electronic Structure and Bonding

According to the composition and the structural pattern, RE_5M_2X must be metallic and the valence electrons must be delocalized. Band calculations were performed to gain more insight into bond strength and electron distribution. Figure 5 shows the total and projected densities of states (PDOS) for Y_5Ni_2Sb. As is typical for electron poor compounds, the Fermi level resides at the low-energy part of the conduction band composed in this case mostly of Y orbitals, with some contribution from Ni orbitals. The bonding contributions from *s* and *p* orbitals of Sb (the most electronegative element) with some mixture of Y orbitals lie at lower energies −13 and −20 eV (out of the presented energy window) separated by gaps from the conduction band. The sharp peak at −10 eV corresponds mainly to contribution of 3*d* Ni orbitals, which are quite localized. The existence of an Y contribution at this region shows covalent mixing of the Y orbitals with the Ni orbitals. On the other hand, the Ni orbitals, mainly *s*-type, interact with the Y orbitals, giving a flat PDOS curve at −9 to −5 eV. The main contribution in this region comes from the Y *d* orbitals that produce most of the states in the vicinity of the Fermi level. According to the calculations Y_5Ni_2Sb and other RE_5M_2X phases should be good metallic conductors.

A complex structure like this presents a variety of distances and bond strengths. Comparisons of the interatomic distances with overlap populations allow one to see where matrix effects, separations fixed by geometric factors, may be more important than bonding in near-neighbor contacts. In cases of matrix effects an application of the empirical Pauling bond-order equation $D(n) = D(1) - 0.6 \log n$ (39), which assigns an order *n* to a bond of distance $D(n)$, is usually quite misleading and calculation of Mulliken overlap populations is preferred. For this purpose, pairwise overlap populations for Y–Y, Y–Ni, and Y–Sb interactions along with the distances in increasing magnitude are listed in Table 6. The corresponding distances from Ho_5Ni_2Sb are given in the last column to simplify the association of the bonds in Y_5Ni_2Sb with the atomic arrangement in the structure. In general, there is a parallel between the electron densities and bond lengths, but some significant deviations assist in highlighting important bonding details. For two Y2–Y2 bonds of 3.423 and 3.856 Å the MOPs are large: 0.374 and 0.246, even when compared to the average MOP of 0.277 in the yttrium metal with the average Y–Y distance of 3.6016 Å. These four Y2 atoms form distorted tetrahedra in slab *II* (Fig. 3), located between the tetragonal antiprisms consisting of Y2 atoms and centered by Sb atoms. The electron density of the bonds inside the tetrahedra is fairly high, which may seem to be rather unusual at the first instance, since these atoms are bound to relatively electronegative Sb atoms. But the Y2 pairs have the Sb neigh-

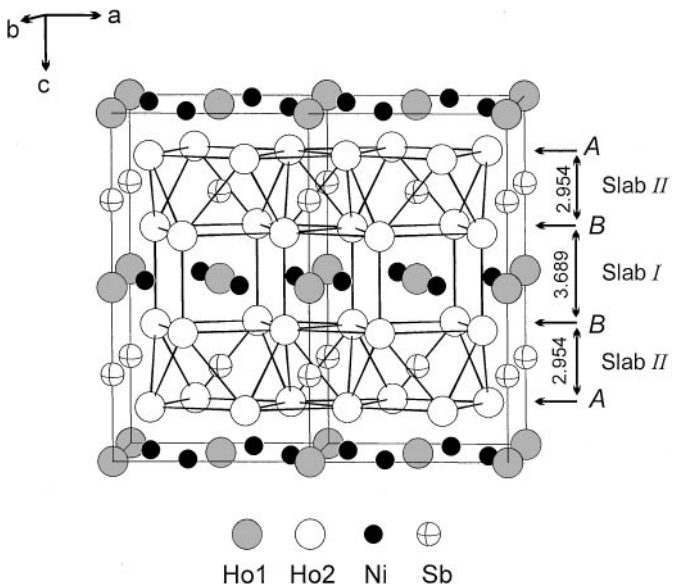

FIG. 2. Structure of Ho_5Ni_2Sb with emphases on the building slabs *I* and *II* and on the distances between $3^2.4.3.4$ Ho nets.

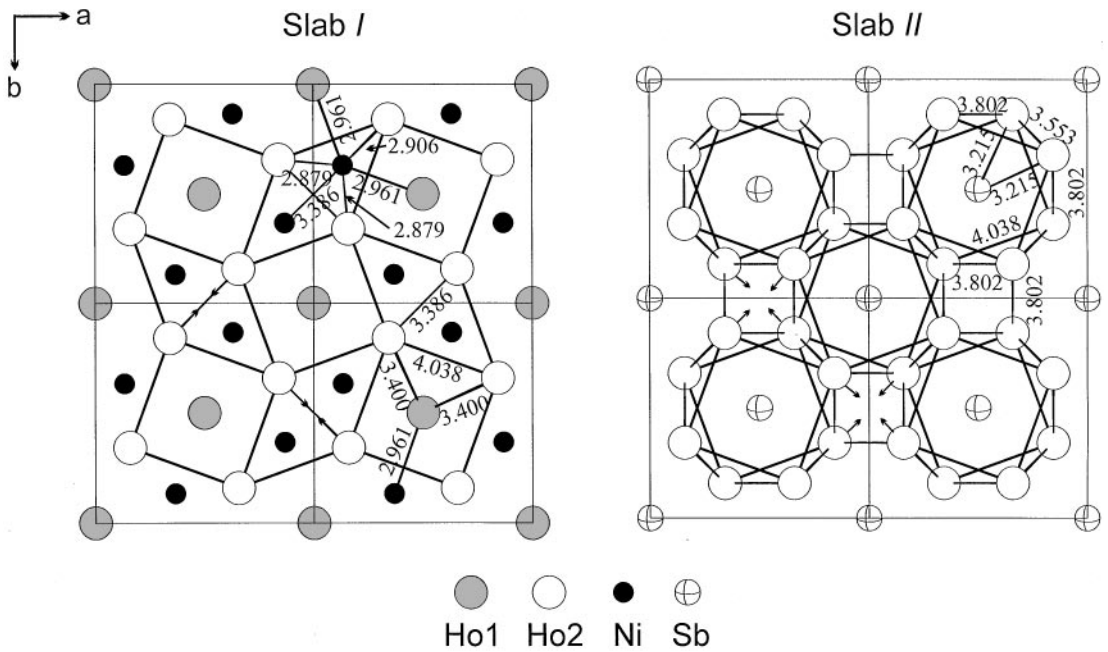

FIG. 3. Projection of slabs *I* and *II* onto the *ab* plane. The arrows show contractions of the Ho2–Ho2 bonds upon substitution of Sb by Bi.

bors only on one side; on the other side there are other Y2 pairs. The energy of these Y2 states is not as high as in the case with Sb on both sides, and more electrons are located in them. This agrees well with the previously discussed tendency of the early transition metals for strong metal–metal interactions, resulting in separate clusters as well as frameworks. Contrarily, a Y2–Y2 pair of 3.605 Å, which bridges two edge-sharing tetragonal antiprisms in slab *II*, has a small MOP of 0.189, which indicates a lower electron concentration and weaker bonding. Now this is not surprising, since this bond is more isolated from the Y2 neighbors and is between two Sb atoms. The fourth Y2–Y2 bond of 3.749 Å reflects the interaction between two yttrium $3^2.4.3.4$ tilings of the same kind, *A* or *B*, and it is fairly strong (MOP = 0.222). There is also bonding between crystallographically different yttrium atoms, which arises from the centering of the Y2 tetragonal prisms by Y1 atoms. Despite being short (3.442 Å) the Y1–Y2 bonds are not the strongest among the Y–Y interactions. The natural assumption is that this distance is moderately to heavily influenced by matrix

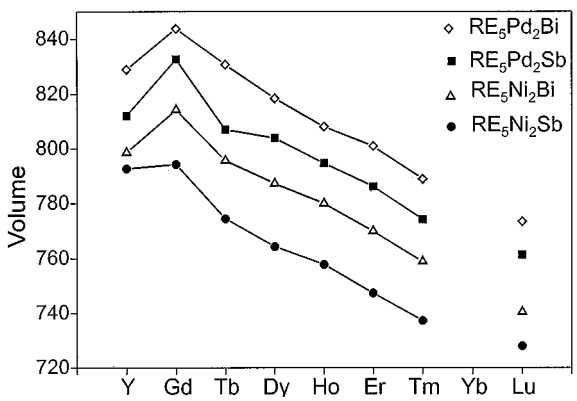

FIG. 4. Unit cell volume (Å^3) versus atomic number for RE_5M_2X.

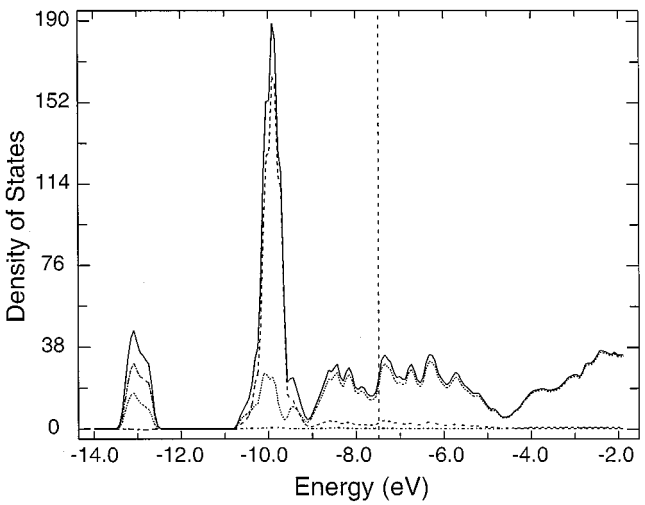

FIG. 5. Total and projected densities of states for Y_5Ni_2Sb. Vertical line represents energy of the Fermi level. Solid line is total DOS; dotted line is Y contribution, dashed line is Ni contribution, and dash-dot line shows Sb contribution.

TABLE 6
Interatomic Distances and MOPs per Atomic Pair for Y_5Ni_2Sb ($a = 7.662$ Å and $c = 13.502$ Å, Atomic Coordinates from Ho_5Ni_2Sb) and Corresponding Distances in Ho_5Ni_2Sb

Bond	No.	Distance in Y_5Ni_2Sb	MOP in Y_5Ni_2Sb	Distance in Ho_5Ni_2Sb
Y1–Y2	32×	3.442	0.232	3.400
Y1–Ni	16×	2.993	0.123	2.961
Y1–Sb	8×	3.375	0.248	3.322
Y2–Y2	8×	3.423	0.374	3.386
Y2–Y2	8×	3.605	0.189	3.553
Y2–Y2	8×	3.749	0.222	3.689
Y2–Y2	16×	3.856	0.246	3.802
Y2–Ni	32×	2.916	0.128	2.879
Y2–Ni	16×	2.944	0.128	2.906
Y2–Sb	32×	3.254	0.304	3.215
Ni–Ni	4×	2.873	−0.066	2.842
Ni–Y2	32×	2.916	0.128	2.879
Ni–Y2	16×	2.944	0.128	2.906
Ni–Y1	16×	2.993	0.123	2.961
Sb–Y2	32×	3.254	0.304	3.215
Sb–Y1	8×	3.375	0.248	3.322

effects. The analysis of the Y–Y bonds shows that the description of the Y2 (Ho2) host structure, based only on geometrical factors, does not reflect strong bonding interactions and is mainly presented to visualize the structural relationship and make the description easier.

There are three kinds of Y–Ni bonds, all of them come from slab *I* and result from the centering of the trigonal Y2 prisms by Ni atoms. The shortest Y2–Ni bond of 2.916 Å has an electron density (MOP = 0.128) similar to that of the largest Y1–Ni bond of 2.993 Å (MOP = 0.123). These Y–Ni interactions are somewhat weaker than the Y–Ni interactions in binary YNi (MOPs are 0.147–0.184 for distances 2.897–2.992 Å). As mentioned above, trigonal prisms with a central late transition metal are characteristic features of the metal-rich pnictides and chalcogenides and the compounds RE_5M_2X are of no exception here. The $Y(2)_6Ni$ prisms joined with the $Y(2)_6Y(1)$ tetragonal prisms shape one part (slab *I*) of the structure, where strong metal–metal bonds seem to play the key role.

The second part (slab *II*) of the structure, composed of Y2 and Sb, has strong Y–Sb bonding and MOP of 0.304 reflects these interactions with interatomic distances of 3.254 Å. There are also interactions of Sb atoms with eclipsed Y1 atoms from the neighboring slabs *I*, but as expected from the bond distances, these interactions are weaker. Except for the bonding in the Y2 tetrahedra, there are no strong dimensionally preferred interactions. This is different from what is often encountered in the early late-transition metal chalcogenides and pnictides, e.g., $Sc_5Ni_2Te_2$ contains channels of Sc atoms filled with Ni atoms (25).

Crystal orbital overlap populations (COOP) were also calculated to gain more insight into different interatomic bonds. The COOP curves of the Y–Y, Y–Ni, and Y–Sb interactions are shown in Fig. 6. The overlap between Y and Sb orbitals is strongly bonding at −13 and −20 eV (out of the given energy window) and becomes slightly antibonding at the Fermi level, the Y–Ni and Y–Y interactions are bonding until −4.8 eV. The Y–Y and Y–Ni bonds contribute significantly to the region at the Fermi level and become even more bonding at the higher energy, around −7 eV. Over −5 eV both interactions are antibonding, especially the Y–Y overlap falls steeply into negative region. Theoretically, introducing more electrons would increase the Y–Ni and Y–Y bonding, while the Y–Sb interactions would remain almost unchanged. The bonding would be optimized for valence electron count of 55 electrons with the bonding–antibonding transition of the Y–Ni and Y–Y states at around −4.8 eV. The valence electron number of 55 per formula unit would correspond to the phases of the same composition with *VIB* elements, the phases with intermediate electron counts from 40 (number of valence electrons per formula unit in RE_5M_2X) to 55 would have *IVB* and *VB* elements instead of rare earths. However, our attempts to synthesize isostructural E_5M_2X compounds, where E = Zr, Hf, Nb, Ta, Mo, W and M = Ni or Co, were unsuccessful.

If the number of electrons is reduced, the Fermi level falls into the slightly antibonding region of the Y–Ni states, which is unfavorable and, besides, reduces the total binding energy of the structure. This observation might explain why we could not obtain holmium antimonides with chromium, manganese, iron, or cobalt.

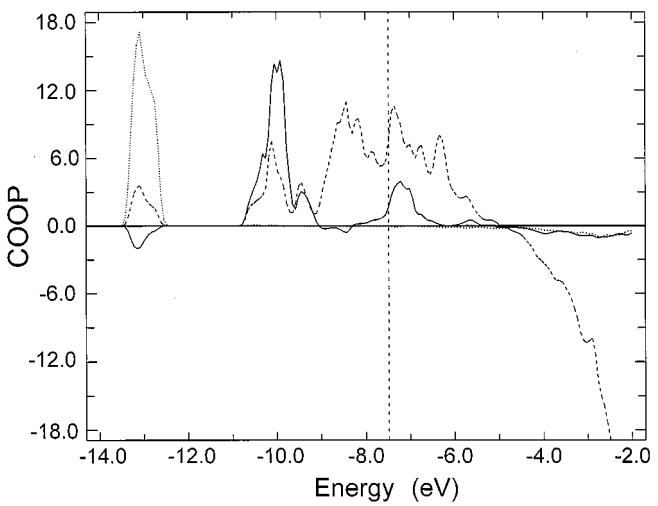

FIG. 6. COOP curves for Y_5Ni_2Sb. Interactions in the upper part are bonding (+), in the lower part antibonding (−). Solid line is Y–Ni interaction, dashed line is Y–Y interaction, and dotted line is Y–Sb interactions.

ACKNOWLEDGMENTS

This research was supported by the Office of the Basic Energy Sciences, Materials Sciences Division, U.S. Department of Energy, DOE. The Ames Laboratory is operated for DOE by Iowa State University under contract No. W-7405-Eng-82. Special thanks are extended to Sasha Pecharsky for collecting powder diffraction data for the Rietveld refinement.

REFERENCES

1. O. Sologub, K. Hiebl, and P. Rogl, *J. Alloys Compd.* **210,** 153 (1994).
2. O. Sologub, K. Hiebl, P. Rogl, and O. I. Bodak, *J. Alloys Compd.* **227,** 40 (1995).
3. O. Sologub, M. Vybornov, P. Rogl, and K.Hiebl, *J. Solid State Chem.* **122,** 266 (1996).
4. K. Hartjes and W. Jeitschko, *J. Alloys Compd.* **226,** 81 (1995).
5. Michael J. Fergunson, Ryan W. Hushagen, and Arthur Mar, *J. Alloys Compd.* **249,** 191 (1997).
6. V. K. Pecharski, Yu. V. Pankevich, and O. I. Bodak, *Sov. Phys. Crystallogr.* **28,** 97 (1983).
7. Petra Wollesen, Wolfgang Jeitschko, Marcus Brylak, and Lutz Dietrich, *J. Alloys Compd.* **245,** L5 (1996).
8. W. K. Hoffman and Wolfgang Jeitschko, *J. Less-Common Met.* **138,** 313 (1988).
9. G. Bolloré, M. J. Fergunson, R. W. Hushagen, and Arthur Mar, *Chem. Mater.* **7,** 2229 (1995).
10. M. Brylak and W. Jeitschko, *Z. Naturforsch. B*: *Chem. Sci.* **50,** 899 (1995).
11. R. A. Gordon, F. J. DiSalvo, and R. Pöttgen, *J. Alloys Compd.* **228,** 16 (1995).
12. A. E. Dwight, *Acta Crystallogr., Sect. B*: *Struct. Crystallogr. Cryst. Chem.* **B33,** 1579 (1977).
13. Yu. Mozharivsky and Yu. B. Kuz'ma, *J. Alloys Compd.* **236,** 203 (1996).
14. A. E. Dwight, *Proc. Rare Earth Res. Conf., 11th, Traverse City, Michigan, 1974*, **2,** 642 (1974).
15. Yu. Mozharivsky and Yu. B. Kuz'ma, *Metally* **4,** 139 (1999).
16. S. I. Mykhalenko, Yu. Mozharivsky, and Yu. B. Kuz'ma, *Dopov. Akad. Nauk Ukr.*, in print.
17. D. Hohnke and E. Parthe, *J. Less-Common Met.* **17,** 291 (1969).
18. L. Brewer and P. R. Wengert, *Metall. Trans.* **4,** 2674 (1973).
19. R. L. Abdon and T. Hughbanks, *J. Am. Chem. Soc.* **117,** 10035 (1995).
20. C. Wang and T. Hughbanks, *Inorg. Chem.* **35,** 6987 (1996).
21. H. Kleinke and H. F. Franzen, *Inorg. Chem.* **35,** 5272 (1996).
22. B. Harbrecht and H. F. Franzen, *J. Less-Common Met.* **113,** 349 (1985).
23. H. Kleinke, *J. Alloys Compd.* **252,** L29 (1997).
24. H. Kleinke, *J. Alloys Compd.* **270,** 136 (1998).
25. P. A. Mggard and J. D. Corbett, *Inorg. Chem.* **38,** 1945 (1999).
26. M. Wang, R. McDonald, and A. Mar, *Inorg. Chem.* **38,** 3435 (1999).
27. M. Koeckerling and H. F. Franzen, *Croatica Chem. Acta* **68**(4), 709 (1995).
28. H. Kleinke and H. F. Franzen, *J. Alloys Compd.* **38,** 68 (1996).
29. H. Kleinke and H. F. Franzen, *J. Alloys Compd.* **255,** 110 (1997).
30. H. Kleinke and H. F. Franzen, *Angew. Chem., Int. Ed. Engl.* **36**(5), 513 (1997).
31. L. G. Akselrud, Yu. M. Grin and P. Yu. Zavalij, "CSD: Universal program package for single crystal and powder data treatment". *Proc. Eur. Crystallogr. Mtg., 12th, Moscow, 1989*, Academy of Sciences, Moscow, USSR (*Kristallogr. Suppl.* **155,** 2 (1989)).
32. J. Rodriguez-Carvajal, "FullProf," Version 3.5, 1997.
33. J. Ren, W. Liang, and M.-H. Whangbo, "Crystal and Electronic Structure Analyzer (CAESAR)." North Carolina State University, Raleigh, NC, 1998.
34. S. Alvarez, "Table of Parameters for Extended Hückel Calculations." Barcelona, 1987.
35. H. Nowotny, E. Dimakopoulou, and H. Kudielka, *Monatsh. Chem.* **88,** 180 (1957).
36. B. Aronsson, *Acta Chem. Scand.* **12,** 31 (1958).
37. E. I. Gladyshevskii and Yu. N. Grin', *Kristallografiya* **26,** 1204 (1981).
38. Yu. B. Kuz'ma, "Kristallochimiya Boridov." Vyshcha Shkola, Lvov, Ukraine, 1983. [in Russian]
39. L. Pauling, "The Chemical Bond." Cornell Univ. Press, Ithaca, NY, 1967.